Int. J. Heat Mass Transfer. Vol. 25, No. 2, pp. 255–266, 1982
Printed in Great Britain

0017 9310/82/020255-12 $03.00/0

TRANSPORT AT LARGE DOWNSTREAM DISTANCES IN MIXED CONVECTION FLOW ADJACENT TO A VERTICAL UNIFORM-HEAT-FLUX SURFACE

VAN P. CAREY
Harrison Radiator Division of General Motors Corporation, Lockport, NY 14094, U.S.A.

and

BENJAMIN GEBHART
Department of Mechanical Engineering and Applied Mechanics, University of Pennsylvania, Philadelphia, PA 19104, U.S.A.

(*Received* 8 *May* 1981 *and in revised form* 24 *July* 1981)

Abstract—A perturbation analysis of mixed convection flow over a vertical semi-infinite surface with uniform heat flux is presented. A matched asymptotic expansion technique is used to construct inner and outer expansions including, for the first time, both mixed convection and higher-order boundary layer effects. It is shown that these effects must be simultaneously included to obtain consistent higher-order approximations to mixed convection boundary layer flow at large downstream distances. Numerical calculations are presented for $Pr = 0.733$ and 6.7 which indicate the relative magnitudes of mixed convection and non-boundary layer effects. In addition, new experimental measurements of surface heat transfer rates and velocity and temperature profiles are presented for mixed convection flow adjacent to a vertical uniform-heat-flux surface in air. The measured profiles are found to be in excellent agreement with those predicted by the analysis. The predicted variation of the Nusselt number is also seen to agree well with the values inferred from the measurements.

NOMENCLATURE

c_p, specific heat;
F_i, terms in the expansion for the stream function ($i = 1, 2, \ldots$);
g, gravitational acceleration;
G^*, $= 5(Gr_x^*/5)^{1/5}$;
Gr_x, $= g\beta x^3(t_0 - t_\infty)/\nu^2$;
Gr_x^*, $= g\beta q x^4/k\nu^2$;
H, $= (t - t_\infty)/\Delta T$;
H_i, terms in the expansion for H ($i = 1, 2, \ldots$);
h_x, local surface heat transfer coefficient;
k, fluid thermal conductivity;
Nu_x, $= h_x x/k$;
p, pressure;
p_∞, total pressure (static + dynamic) far from the surface;
P_i, terms in the inner expansion for $p - p_\infty$ ($i = 1, 2, \ldots$);
$\bar{P}_i$, terms in the outer expansion for $p - p_\infty$ ($i = 1, 2, \ldots$);
Pr, Prandtl number;
q, surface heat flux;
r, radial distance measured from the leading edge;
$\bar{R}$, $= u_\infty(5k\nu^2/g\beta q)^{1/4}/\nu$;
Re_x, $= u_\infty x/\nu$;
t, temperature;
t_0, surface temperature;
t_∞, ambient temperature;
u, velocity in the x direction;
u_∞, free stream velocity;
U, $= \nu G^{*2}/5x$;
v, velocity in the y direction;
x, coordinate parallel to the surface;
X, $= (k\nu^2/g\beta q)^{1/4}/5$;
y, coordinate normal to the surface.

Greek symbols

β, coefficient of thermal expansion;
δ, $= 5x/G^*$;
ΔT, $= q\delta/k$;
ε_H, $= 5/G^*$;
ε_M, $= \bar{R}/(G^*/5)^{3/4}$;
η, $= y/\delta$;
θ, $= \tan^{-1}(y/x)$;
μ, absolute viscosity;
ν, kinematic viscosity;
ρ, local fluid density;
ρ_∞, density of the ambient fluid;
τ_w, surface shear stress;
$\bar{\psi}_i$, terms in the outer expansion for Ψ ($i = 1, 2, \ldots$);
Ψ, stream function.

1. INTRODUCTION

IN TECHNOLOGY and the environment, external boundary layer flows often occur in which both buoyancy and motion of the ambient fluid have strong effects on the resulting convective transport. Such mixed convection flows have been the subject of numerous studies. Most previous studies of laminar mixed convection flows past vertical flat surfaces have considered either an isothermal or a uniform-heat-flux

surface in a uniform external stream. Since similarity solutions cannot be obtained for these flow circumstances, analysis of these flows requires more powerful techniques, such as finite difference numerical schemes, local similarity analysis or perturbation methods.

Merkin [1] points out that for the two effects in the same direction, the flow near the leading edge of an isothermal surface is mostly forced convection flow, since thermal transport is not yet established. The buoyancy effect grows downstream, until at large downstream distances, the flow behavior approaches that of pure free convection flow. For opposed effects, the flow near the leading edge is again mostly forced convection. However, the increasing effect of the opposed buoyancy force with downstream distance eventually decelerates and reverses the flow near the surface. This amounts to a flow separation. Thus opposed effects result in the possibility of flow separation. Similar considerations apply to mixed convection flow adjacent to a uniform-heat-flux surface. Earlier studies of mixed convection flow near an isothermal surface by Eshghy [2] and Szewczyk [3] did not address these physical considerations. In addition, Merkin [1] points out that, for the isothermal surface condition, expansions at large downstream distances should contain logarithmic terms. These were not included in the solutions of Eshghy [2] or Szewczyk [3].

Most past studies of mixed convection flow over vertical surfaces have considered the flow at small to moderate distances from the leading edge, where the buoyancy force effects are of the same order or smaller than forced-flow effects; that is, $Gr_x/Re_x^2 \leq O(1)$. These include the studies of Sparrow and Gregg [4], Kliegel [5], Lloyd and Sparrow [6], Oosthuizen and Hart [7], Wilks [8], Gryzagoridis [9], Hommel [10], and Afzal and Banthiya [11]. In a few of these investigations, such as Oosthuizen and Hart [7] and Afzal and Banthiya [11], results are presented at fairly large downstream distances. However, the most thorough analyses of the asymptotic behavior of mixed convection flow over a vertical surface at large downstream distances, are those of Merkin [1] for the isothermal surface and Wilks [12] for the uniform-heat-flux surface. For aiding effects, Merkin [1] obtained expansions for the solution near the leading edge and far downstream. The gap between these solutions was bridged with a numerical marching scheme. Forced convection flow with opposed thermal buoyancy was also analyzed up to the point of separation. For both circumstances, computed results were presented for $Pr = 1$. For aiding flow, the expansions at large downstream distances include the logarithmic terms omitted by Szewczyk [3] and Eshghy [2].

Similarly, Wilks [12] obtained expansions for the solution near the leading edge and far downstream for mixed convection along a vertical uniform-heat-flux surface in a uniform free stream. The solution at intermediate distances was determined using a numerical marching technique. Wilks [12] showed that for the uniform-flux surface, no logarithmic terms arise.

Despite these studies, there are aspects of mixed convection flow along vertical surfaces at large downstream distances which warrant further investigation. The expansions obtained by Merkin [1] and Wilks [12] contain terms up to second order in the perturbation parameter. This is mathematically appropriate when the boundary layer equations are assumed to be the valid governing equations of motion. However, from a physical standpoint, the contributions of the second order terms, relating to mixed convection, may be small compared with the contributions of terms in the Navier–Stokes equations which were discarded when making the boundary layer approximations. Hence, including 2nd-order terms may be physically inconsistent. It is necessary to simultaneously assess both the effects of non-zero free stream velocity and of higher-order corrections to boundary layer analysis.

There is also another difficulty with the analysis of Wilks [12]. There is an error in the 1st order correction equation for the expansions at large downstream distances. Apparently, the computed results for large downstream distances were based on this erroneous equation.

Although considerable time has elapsed since the studies of Merkin [1] and Wilks [12], the asymptotic behavior of mixed convection flows at large downstream distances has not been explored experimentally. In fact, there is very little experimental data concerning the behavior of mixed convection flow over vertical surfaces even at small downstream distances. The very early heat transfer measurements of Kliegel [5] apply to forced flow perturbed with thermal buoyancy. In a later study, Gryzagoridis [9] measured surface heat transfer rates and velocity and temperature profiles in mixed convection flow adjacent to a vertical isothermal surface in a uniform free stream. The measurements were largely in flows in which the buoyancy effects are the same order as, or smaller than, forced convection effects. The measured surface heat transfer rates and temperature profiles agreed well with the analytical studies of Lloyd and Sparrow [6] and Oosthuizen and Hart [7]. However, the measured velocity profiles were found to be in poor agreement with these calculations. No other data has been found in the literature for mixed convection flow over vertical surfaces.

The present study resolves the matter of consistent higher-order approximations of the downstream behavior of mixed convection flow adjacent to a vertical uniform-heat-flux surface in a uniform free stream. Transport behavior far downstream is of considerable interest, since it is the foundation for studies of the stability and transition of such flows. Here the method of matched asymptotic expansions is used to construct solutions valid far downstream (ε_H and ε_M small). The non-zero free stream velocity and higher-order boun-

dary layer effects are considered simultaneously as perturbations of the associated pure free convection flow. It will be seen that a boundary layer correction term will enter the expansions before the 2nd-order correction term for mixed convection reported by Wilks [12]. Computed results are presented for Prandtl numbers, Pr, of 0.733 and 6.7.

These results are then compared with new experimental measurements of surface heat transfer rates and velocity and temperature profiles in such a mixed convection flow. The experimental results will be seen to agree extremely well with those predicted by the analysis.

2. ANALYSIS

The formulation relates to a semi-infinite vertical surface with the origin at the leading edge. The x axis is vertically upward and the y axis is normal to the surface. Heat is dissipated uniformly, at the surface, to the fluid. Employing the Boussinesq approximations and neglecting the viscous dissipation and pressure terms in the energy equation, the 2-dim. governing equations for steady flow are:

$$\frac{\partial u}{\partial x} + \frac{\partial v}{\partial y} = 0, \tag{1}$$

$$u\frac{\partial u}{\partial x} + v\frac{\partial u}{\partial y} = \nu\left(\frac{\partial^2 u}{\partial x^2} + \frac{\partial^2 u}{\partial y^2}\right) + g\beta(t - t_\infty) - \frac{1}{\rho}\frac{\partial p}{\partial x}, \tag{2}$$

$$u\frac{\partial v}{\partial x} + v\frac{\partial v}{\partial y} = \nu\left(\frac{\partial^2 v}{\partial x^2} + \frac{\partial^2 v}{\partial y^2}\right) - \frac{1}{\rho}\frac{\partial p}{\partial y}, \tag{3}$$

$$u\frac{\partial t}{\partial x} + v\frac{\partial t}{\partial y} = \frac{\nu}{Pr}\left(\frac{\partial^2 t}{\partial x^2} + \frac{\partial^2 t}{\partial y^2}\right). \tag{4}$$

Here, u and v are velocity components in the x and y directions respectively, ν is the kinematic viscosity, ρ is the fluid density, t is temperature, p is pressure, g is the gravitational acceleration, β is the coefficient of thermal expansion, and Pr is the Prandtl number. The corresponding boundary conditions are:

$$u = v = 0, \quad \frac{\partial t}{\partial y} = \frac{-q}{k} \quad \text{at } y = 0,\ x \geq 0, \tag{5}$$

$$\frac{\partial u}{\partial y} = v = 0, \quad \frac{\partial t}{\partial y} = 0 \quad \text{at } y = 0,\ x < 0, \tag{6}$$

$$u \sim u_\infty,\ t \sim t_\infty,\ p \sim p_\infty - \frac{1}{2}\rho u_\infty \quad \text{as } y \to \infty \text{ and upstream.} \tag{7}$$

Here q and k are the surface heat flux and thermal conductivity respectively. The non-boundary layer and mixed convection effects may decay differently, in the asymptotic sense with increasing downstream distance. Using the method of matched asymptotic expansions, two different perturbation parameters may be expected to arise: one characterizing higher-order corrections to boundary layer theory, ε_H, and the other characterizing mixed convection effects, ε_M. Defining a streamfunction Ψ so that $u = \Psi_y$ and $v = -\Psi_x$, the inner and outer expansions are taken as:

inner

$$\Psi = U\delta[F_0(\eta) + \varepsilon_M F_1(\eta) + \varepsilon_H F_2(\eta) + \varepsilon_M^2 F_3(\eta) + \varepsilon_M\varepsilon_H F_4(\eta) + \ldots], \tag{8}$$

$$t - t_\infty = \Delta T[H_0(\eta) + \varepsilon_M H_1(\eta) + \varepsilon_H H_2(\eta) + \varepsilon_M^2 H_3(\eta) + \varepsilon_M\varepsilon_H H_4(\eta) + \ldots], \tag{9}$$

$$p - p_\infty = -\frac{1}{2}\rho u_\infty^2 + \rho U^2[\varepsilon_M\varepsilon_H P_1(\eta) + \ldots]. \tag{10}$$

outer

$$\Psi = \bar{\psi}_0 + \bar{\psi}_1 + \bar{\psi}_2 + \ldots, \tag{11}$$

$$t - t_\infty = \bar{T}_0 + \bar{T}_1 + \bar{T}_2 + \ldots, \tag{12}$$

$$p - p_\infty = -\frac{1}{2}\rho u_\infty^2 + \bar{P}_1 + \bar{P}_2 + \ldots, \tag{13}$$

where

$$U = \nu G^{*2}/5x,\ \delta = 5x/G^*,\ \Delta T = q\delta/k, \tag{14}$$

$$\eta = y/\delta,\ G^* = 5(Gr_x^*/5)^{1/5},\ Gr_x^* = (g\beta q x^4/k\nu^2). \tag{15}$$

The form of the inner expansion (10) for $p - p_\infty$ is chosen so that it can be matched in a consistent manner with the pressure field in the outer inviscid flow. Based on the results of Mahajan and Gebhart [13] and Wilks [12], who studied these effects separately, ε_H and ε_M are defined as

$$\varepsilon_H = 5/G^*,\ \varepsilon_M = \bar{R}/(G^*/5)^{3/4}, \tag{16a}$$

where

$$\bar{R} = \frac{u_\infty}{\nu}(5k\nu^2/g\beta q)^{1/4} = Re_x/(Gr_x^*/5)^{1/4}. \tag{16b}$$

Hence,

$$\varepsilon_M = \bar{R}\varepsilon_H^{3/4} \tag{17}$$

For the ranges of u_∞ and q considered here, $\bar{R}$ is an $O(1)$ constant, which implies that $Re_x = O([Gr_x^*/5]^{1/4})$. Substituting (17) into (8) through (10), the inner expansions become:

inner

$$\Psi = U\delta[F_0(\eta) + \bar{R}\varepsilon_H^{3/4} F_1(\eta) + \varepsilon_H F_2(\eta) + \bar{R}^2\varepsilon_H^{3/2} F_3(\eta) + \bar{R}\varepsilon_H^{7/4} F_4(\eta) + \ldots], \tag{18}$$

$$t - t_\infty = \Delta T[H_0(\eta) + \bar{R}\varepsilon_H^{3/4} H_1(\eta) + \varepsilon_H H_2(\eta) + \bar{R}^2\varepsilon_H^{3/2} H_3(\eta) + \bar{R}\varepsilon_H^{7/4} H_4(\eta) + \ldots], \tag{19}$$

$$p - p_\infty = -\frac{1}{2}\rho u_\infty^2 + \rho U^2[\bar{R}\varepsilon_H^{7/4} P_1(\eta) + \ldots]. \tag{20}$$

In the inner region, from (18) it is seen that

$$u = U[F_0' + \bar{R}\varepsilon_H^{3/4} F_1' + \varepsilon_H F_2' + \bar{R}^2\varepsilon_H^{3/2} F_3' + \bar{R}\varepsilon_H^{7/4} F_4' + \ldots]. \quad (21)$$

In the usual manner for matched asymptotic expansions, the expansions in (18), (19) and (20) are substituted into the governing equations. Perturbation equations are then obtained by collecting terms with like powers of ε_H. Successive matching in the manner described by Van Dyke [14] yields the boundary conditions for each level of the expansions in the inner and outer regions. The matching considerations here are virtually the same as those of Mahajan and Gebhart [13] and therefore will not be discussed in detail. After matching, it is found that the terms of the inner expansion, up to F_4, must satisfy:

$$F_0''' - 3F_0'^2 + 4F_0F_0'' + H_0 = 0, \quad (22a)$$

$$H_0'' + Pr(4F_0H_0' - F_0'H_0) = 0, \quad (22b)$$

$$F_0(0) = F_0'(0) = H_0'(0) + 1 = F_0'(\infty) = H_0(\infty) = 0, \quad (22c)$$

$$F_1''' + F_1F_0'' + 4F_0F_1'' - 3F_0'F_1' + H_1 = 0, \quad (23a)$$

$$H_1'' + Pr(2F_0'H_1 - F_1'H_0 + 4F_0H_1' + H_0'F_1) = 0, \quad (23b)$$

$$F_1(0) = F_1'(0) = H_1'(0) = H_1(\infty) = F_1'(\infty) - \frac{1}{5} = 0, \quad (23c)$$

$$F_2''' + 4F_0F_2'' - 2F_2'F_0' + H_2 = 0, \quad (24a)$$

$$H_2'' + Pr(3F_0'H_2 - H_0F_2' + 4F_0H_2') = 0, \quad (24b)$$

$$F_2(0) = F_2'(0) = H_2'(0) = H_2(\infty) = F_2'(\infty) - \frac{4}{5}A_0\cot\frac{\pi}{5} = 0, \quad (24c)$$

$$F_3''' + 4F_0F_3'' - 2F_3F_0'' + F_1F_1'' + H_3 = 0, \quad (25a)$$

$$H_3'' + Pr(5F_0'H_3 + 2F_1'H_1 - H_0F_3' + 4F_0H_3' + F_1H_1' - 2H_0'F_3) = 0, \quad (25b)$$

$$F_3(0) = F_3'(0) = H_3'(0) = F_3'(\infty) = H_3(\infty) = 0, \quad (25c)$$

$$F_4''' + F_0'F_4' + F_1'F_2' + 4F_0F_4'' + F_1F_2'' - 3F_0''F_4 + H_4 = \frac{4}{25}A_0\cot\frac{\pi}{5}, \quad (26a)$$

$$H_4'' + Pr(6F_0'H_4 + 3F_1'H_2 + 2H_1F_2' - H_0F_4' + 4F_0H_4' + F_1H_2' - 3H_0'F_4) = 0, \quad (26b)$$

$$P_1' = 0, \quad (26c)$$

$$F_4(0) = F_4'(0) = H_4'(0) = H_4(\infty) = 0, \quad (26d)$$

$$F_4'(\infty) = \frac{-1}{5}A_1\cot\frac{\pi}{5}, \quad P_1(\infty) = \frac{-4}{25}A_0\cot\frac{\pi}{5}, \quad (26e)$$

where

$$F_0(\infty) = A_0, \; F_1(\infty) = \frac{1}{5}\eta + A_1.$$

In the outer inviscid region, ψ_0 is simply the contribution due to the uniform free stream, $\psi_0 = u_\infty y = u_\infty r\sin\theta$. From matching, the higher-order terms in the outer expansion for Ψ must satisfy:

$$\nabla^2\bar{\psi}_1 = 0, \quad \text{at } \theta = \pi: \; \bar{\psi}_1 = 0, \quad \text{at } \theta = 0: \; \bar{\psi}_1 = \nu A_0(r/X)^{4/5}, \quad (27)$$

$$\nabla^2\bar{\psi}_2 = 0, \quad \text{at } \theta = \pi: \; \bar{\psi}_2 = 0, \quad \text{at } \theta = 0: \; \bar{\psi}_2 = 5^{3/4}\nu\bar{R}A_1(r/X)^{1/5}, \quad (28)$$

$$\nabla^2\bar{\psi}_3 = 0, \quad \text{at } \theta = \pi: \; \bar{\psi}_3 = 0, \quad \text{at } \theta = 0: \; \bar{\psi}_3 = 5\nu A_2, \quad (29)$$

$$\nabla^2\bar{\psi}_4 = 0, \quad \text{at } \theta = \pi: \; \bar{\psi}_4 = 0, \quad \text{at } \theta = 0: \; \bar{\psi}_4 = 5^{3/2}A_3\bar{R}^2\nu(r/X)^{-2/5}, \quad (30)$$

where $X = (1/5)(k\nu^2/g\beta q)^{1/4}$, $F_2(\infty) = (4/5)(A_0\eta\cot\pi/5 + A_2)$, and $A_3 = F_3(\infty)$. Solving these equations using Bernoulli's equation to obtain terms in the expansion for pressure, yields, for the outer region:

$$\bar{T}_0 = \bar{T}_1 = \bar{T}_2 = \bar{T}_3 = \bar{T}_4 = 0, \quad (31)$$

$$\bar{\psi}_0 = u_\infty r\sin\theta, \; \bar{\psi}_1 = \frac{\nu A_0}{\sin 4\pi/5}\left(\frac{r}{X}\right)^{4/5} \times \sin\frac{4}{5}(\pi - \theta), \quad (32a)$$

$$\bar{\psi}_2 = \frac{5^{3/4}\nu\bar{R}A_1}{\sin\pi/5}\left(\frac{r}{X}\right)^{1/5}\sin\frac{1}{5}(\pi - \theta), \quad (32b)$$

$$\bar{\psi}_3 = 5\nu A_2\left(1 - \frac{\theta}{\pi}\right), \; \bar{\psi}_4 = \frac{5^{3/2}\nu\bar{R}^2A_3}{\sin 2\pi/5}\left(\frac{r}{X}\right)^{-2/5}\sin\frac{2}{5}(\pi - \theta), \quad (32c)$$

$$\bar{P}_1 = -\frac{4}{5}\rho\frac{A_0u_\infty}{\sin\pi/5}\left(\frac{\nu}{X}\right)\left(\frac{X}{r}\right)^{1/5}\cos\frac{1}{5}(\theta - \pi), \quad (33a)$$

$$\bar{P}_2 = -\frac{1}{2}\rho\frac{(4A_0/5)^2}{\sin^2\pi/5}\left(\frac{\nu}{X}\right)^2\left(\frac{X}{r}\right)^{2/5}. \quad (33b)$$

For the inner expansions, eigenfunctions also exist which identically satisfy the boundary conditions at zero and infinity. A combination of these may be added to the solution which will still satisfy all the conditions imposed. The eigenfunction terms associated with expansions (18) and (19) are of the forms $C_n\varepsilon_H^{\lambda_n}f_n(\eta)$ and $C_n\varepsilon_H^{\lambda_n}\phi_n(\eta)$, respectively. C_n is a multiplicative constant associated with the stream function upstream, and λ_n is the corresponding eigenvalue. The lowest order eigenfunctions associated with the inner expansions are:

$$f_1 = 4F_0 - \eta F_0', \quad (34)$$

$$\phi_1 = H_0 - \eta H_0', \quad (35)$$

with the corresponding eigenvalue, λ_1, equal to 5/4. These are identical to the lowest order eigenfunctions found by Mahajan and Genhart [13] for the pure free convection case. Other eigenvalues found for the inner expansion have values greater than 2 and hence will not appear in expansions (18) and (19) to $O(\varepsilon_H^{7/4})$.

Eigenfunctions of the type described above must be

considered when obtaining a series solution valid far downstream in a boundary layer flow. In several such flows, Stewartson [15] has found that an inconsistency arises in the large η behavior of the solution, when a term in the postulated series is the same order as one of the eigenfunctions. Stewartson [15] also showed that the inconsistency could be resolved by inserting a log or loglog term into the series. As discussed in the previous section, Merkin [1] obtained a series solution, valid far downstream, for mixed convection flow adjacent to a vertical isothermal surface. For that flow circumstance, Merkin [1] encountered a situation similar to that described by Stewartson [15]. The lowest order eigenfunction was found to be the same order as one of the terms in the expansions, resulting in an inconsistency in the large η behavior at that level. Merkin [1] resolved the inconsistency by inserting logarithmic terms in the expansions for the temperature and stream functions.

For the uniform-heat-flux surface condition, the lowest-order eigenvalue ($\lambda_1 = 5/4$) is not equal to the exponent of ε_H in any of the terms in expansions (18) and (19). No inconsistencies exist in the large η behavior of $F_i(\eta)$ and $H_i(\eta)$ for $i = 0$–4. Hence, for expansions (18) and (19), to $O(\varepsilon_H^{7/4})$, inclusion of a log term is not appropriate. In Merkin's [1] expansions for the corresponding problem with an isothermal surface, the appearance of log terms at an early stage is apparently a consequence of the way in which the surface temperature and the perturbation parameter vary with x.

From a global energy balance it may easily be shown that the contribution of the lowest order eigenfunctions to the expansions (18) and (19) must be identically zero. Details of the procedure may be found in Mahajan and Gebhart [13]. It is thus concluded that inner expansions (18) through (20) are appropriate up to $O(\varepsilon_H^{7/4})$.

The inner region equations (22)–(26) were solved for $Pr = 0.733$ and $Pr = 6.7$ using a predictor–corrector shooting method. Values of $F_i''(0)$ and $H_i(0)$, $i = 1$–4, were guessed and subsequently corrected to satisfy the far boundary conditions. A fixed step size of $\Delta\eta = 0.05$ was used while integrating from $\eta = 0$ to $\eta = \eta_{edge}$. For $Pr = 0.733$, $\eta_{edge} = 20$ was used, while for $Pr = 6.7$, η_{edge} was taken to be 35. The resulting values of $F_i''(0)$ and $H_i(0)$ and other numerical data of interest are summarized in Table 1 for $Pr = 0.733$ and $Pr = 6.7$. The velocity and temperature profiles associated with the above solutions are shown in Figs. 1–4. From (26c) and (26e) it is seen that

$$P_1 = \text{constant} = \frac{-4}{25} A_0 \cot\frac{\pi}{5}. \tag{36}$$

The local temperature difference, Nusselt number, and surface shear stress are:

$$t_0 - t_\infty = \frac{q\delta}{k} H_0(0)\left(1 + \bar{R}\varepsilon_H^{3/4}\frac{H_1(0)}{H_0(0)} + \varepsilon_H\frac{H_2(0)}{H_0(0)} + \bar{R}^2\varepsilon_H^{3/2}\frac{H_3(0)}{H_0(0)} + \bar{R}\varepsilon_H^{7/4}\frac{H_4(0)}{H_0(0)} + \ldots\right), \tag{37}$$

$$Nu_x = \frac{h_x x}{k} = \frac{1}{\varepsilon_H H_0(0)}\left\{1 - \bar{R}\varepsilon_H^{3/4}\frac{H_1(0)}{H_0(0)} - \varepsilon_H\frac{H_2(0)}{H_0(0)} - \bar{R}^2\varepsilon_H^{3/2}\left[\frac{H_3(0)}{H_0(0)} - \left(\frac{H_1(0)}{H_0(0)}\right)^2\right] - \bar{R}\varepsilon_H^{7/4} \times \left[\frac{H_4(0)}{H_0(0)} - 2\frac{H_1(0)H_2(0)}{[H_0(0)]^2}\right] + \ldots\right\}, \tag{38}$$

$$\tau_w = \rho\nu\frac{U}{\delta}F_0''(0)\left(1 + \bar{R}\varepsilon_H^{3/4}\frac{F_1''(0)}{F_0''(0)} + \varepsilon_H\frac{F_2''(0)}{F_0''(0)} + \bar{R}^2\varepsilon_H^{3/2}\frac{F_3''(0)}{F_0''(0)} + \bar{R}\varepsilon_H^{7/4}\frac{F_4''(0)}{F_0''(0)} + \ldots\right), \tag{39}$$

where h_x is the local heat transfer coefficient and τ_w is the surface shear stress.

Substituting for the different Prandtl numbers yields:

for $Pr = 0.733$:

$$t_0 - t_\infty = \frac{q\delta}{k} H_0(0)(1 - 0.06439\bar{R}\varepsilon_H^{3/4} - 0.24423\varepsilon_H - 0.00430\bar{R}^2\varepsilon_H^{3/2} + 0.40261\bar{R}\varepsilon_H^{7/4} + \ldots), \tag{40a}$$

$$Nu_x = \frac{1}{\varepsilon_H H_0(0)}(1 + 0.06439\bar{R}\varepsilon_H^{3/4} + 0.24423\varepsilon_H + 0.00844\bar{R}^2\varepsilon_H^{3/2} - 0.37116\bar{R}\varepsilon_H^{7/4} + \ldots), \tag{40b}$$

$$\tau_w = \rho\nu\frac{U}{\delta}F_0''(0)(1 - 0.02745\bar{R}\varepsilon_H^{3/4} - 0.10334\varepsilon_H + 0.01461\bar{R}^2\varepsilon_H^{3/2} + 0.18386\bar{R}\varepsilon_H^{7/4} + \ldots); \tag{40c}$$

Table 1. Computed constants for mixed convection flow adjacent to a vertical uniform-heat-flux surface

i	$F_i''(0)$		$H_i(0)$		A_i	
	$Pr = 0.733$	$Pr = 6.7$	$Pr = 0.733$	$Pr = 6.7$	$Pr = 0.733$	$Pr = 6.7$
0	0.808931	0.356332	1.479807	0.841701	0.507506	0.205833
1	−0.022209	0.006178	−0.095286	−0.054026	−0.45744	−0.55057
2	−0.083596	0.006691	−0.361412	−0.08258	−1.10914	−0.53744
3	0.011820	0.005962	−0.0063594	−0.03246	0.07002	0.27064
4	0.148733	0.006178	0.595782	0.35555		

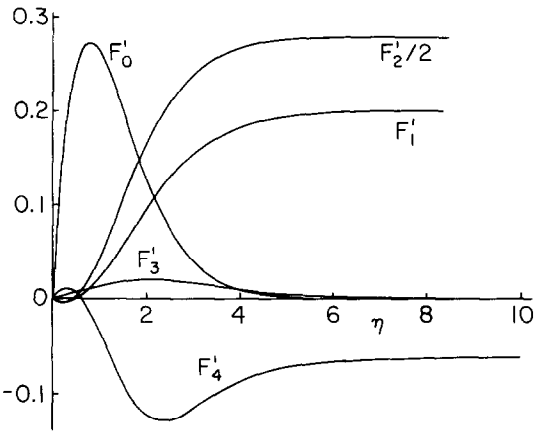

FIG. 1. Velocity function distributions for $Pr = 0.733$.

for $Pr = 6.7$:

$$t_o - t_\infty = \frac{q\delta}{k} H_0(0)(1 - 0.06419\bar{R}\varepsilon_H^{3/4} - 0.09811\varepsilon_H - 0.03856\bar{R}^2\varepsilon_H^{3/2} + 0.42242\bar{R}\varepsilon_H^{7/4} + \ldots), \quad (41a)$$

$$Nu_x = \frac{1}{\varepsilon_H H_0(0)}(1 + 0.06419\bar{R}\varepsilon_H^{3/4} + 0.09811\varepsilon_H + 0.04268\bar{R}^2\varepsilon_H^{3/2} - 0.40982\bar{R}\varepsilon_H^{7/4} + \ldots), \quad (41b)$$

$$\tau_w = \rho\nu\frac{U}{\delta}F_0''(0)(1 + 0.01734\bar{R}\varepsilon_H^{3/4} + 0.01878\varepsilon_H + 0.01673\bar{R}^2\varepsilon_H^{3/2} + 0.01734\bar{R}\varepsilon_H^{7/4} + \ldots). \quad (41c)$$

It is interesting to note that the first correction due to mixed convection effects and the first correction due to non-boundary layer effects both affect $t_o - t_\infty$, Nu_x and τ_w in the same manner.

In the inner expansions, (18)–(21), and in the terms of the outer expansions, (31)–(33), note that $\bar{R}$ appears as a factor in terms which result from mixed con-

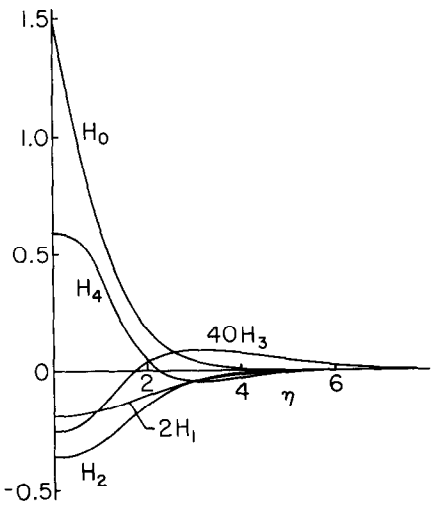

FIG. 2. Temperature function distributions for $Pr = 0.733$.

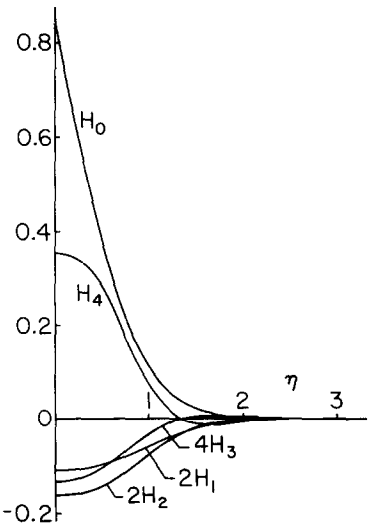

FIG. 4. Temperature function distributions for $Pr = 6.7$.

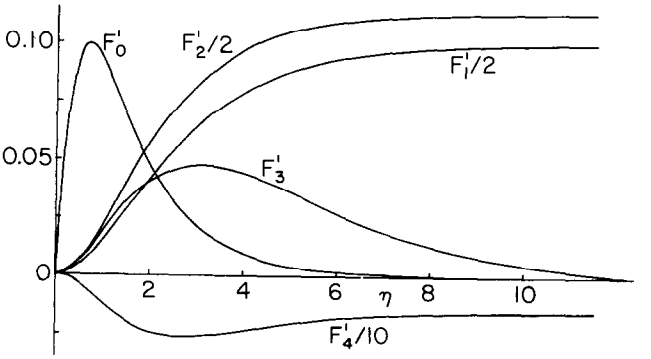

FIG. 3. Velocity function distributions for $Pr = 6.7$.

vection effects. Terms in which $\bar{R}$ does not appear, are due to higher-order boundary layer effects alone. In the inner expansions, (18)–(21), and in (37)–(41), the terms of $O(\bar{R}\varepsilon_H^{3/4})$ and $O(\bar{R}^2\varepsilon_H^{3/2})$ are purely a consequence of mixed convection effects. These terms are equivalent to the 1st- and 2nd-order corrections reported by Wilks [12]. The term of $O(\varepsilon_H)$ is due to higher-order boundary-layer effects alone. This term is the 1st-order correction reported by Mahajan and Gebhart [13]. The term of $O(\bar{R}\varepsilon_H^{7/4})$ is a cross term representing interaction of mixed-convection and non-boundary layer effects. As $\bar{R} \to 0$, the inner and outer expansions reduce to the expansions obtained by Mahajan and Gebhart [13] for higher-order effects in pure natural convection flow.

Using the method of matched asymptotic expansions, consistent higher-order approximations for the flow and transport in the inner region are obtained here to $O(\varepsilon_H^{7/4})$. In addition, the outer solutions indicate the higher-order changes in the outer inviscid flow which result from modification of the flow in the inner region by mixed-convection effects.

In contrast, the coordinate expansion technique used by both Merkin [1] and Wilks [12] does not include higher-order boundary layer effects of comparable magnitude. It also provides no information regarding the outer inviscid flow behavior. Thus, the method of matched asymptotic expansions is here more physically consistent, and it provides more information about the flow than simple coordinate expansion techniques. Upon converting results of the present analysis for $Pr = 1$ to the formulation of Wilks [12], it was found that the error in [12] had only a small effect on the resulting solutions.

3. EXPERIMENTS IN AIR

To assess the accuracy of the analysis presented in the previous section, experimental measurements were made in the mixed convection flow adjacent to a vertical uniform-heat-flux surface in air. The experimental system is shown in Fig. 5. The experiments were conducted in a cylindrical test section 33.7 cm in inside diameter and 76.2 cm in height. The heated surface was formed by stretching a 15 cm wide piece of 0.0127 mm thick Inconel 600 foil in a special support fixture. The jaws at the top of the fixture were spring loaded so that they exerted an upward force on the foil. The foil was looped around an aluminum support covered with plastic tape. This support resisted the upward pull of the jaws and thereby pulled the foil tight. A 0.64 cm thick piece of foam insulation was inserted between the two sections of foil, so that at steady state, all heat dissipated by the foil was transferred outward to the surrounding air. The resulting assembly formed a plate 15 cm wide, 40 cm long and 0.64 cm thick, with a front and back surface of the Inconel foil and an interior of foam insulation. The lower aluminum support provided a smooth leading edge configuration. Passing electric current through the foil provided a uniform-heat-flux surface condition.

Prior to the experiments, the surface was aligned vertically, with the leading edge horizontal, using a plumb line and level. Air flow was supplied to the test section by a line from a compressed air storage tank. The storage tank was maintained at about 7 atm pressure by a system which compressed and dehumidified the air. Air from the storage tank was sent through a pressure regulator, a critical orifice flow meter and then into the test section. The system had a peak flow capacity of about 0.7 m^3/s at 1 atm pressure. This amounted to a peak mean velocity of 7.5 cm/s in the test section. By maintaining critical flow conditions at the orifice in the orifice meter, the flow through the test section was a function only of the pressure upstream of the meter. The pressure there was held within ± 0.07 atm (± 7 kPa) by the pressure regulator. The flow through the test section was thereby held constant within ± 0.05 cm/s. Measurements indicated that the temperature of the air supplied to the test section did not vary by more than ± 0.05°C during a test. These tolerances could be held for as long as 45 min, despite cycling of the compressor to maintain the supply in the storage tank. The air flow rate was measured with the critical orifice meter as a rough check of the hot wire measurements of the mean flow in the test section.

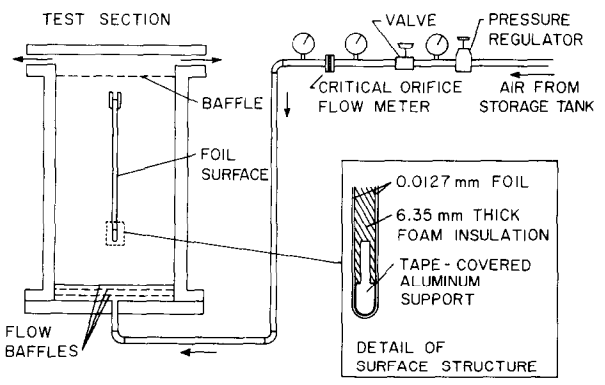

FIG. 5. System used for mixed convection experiments.

Large-pressure-drop baffles were inserted at the top and bottom of the test section to ensure uniform flow distribution over the test section. Hot-wire measurements across the test section, made before inserting the surface, indicated that the flow was uniform to within ± 0.10 cm/s. During the experiments, the variation of the core velocity with vertical location was found to be negligible. The usual acceleration of the core flow which occurs in the entrance of a pipe was not appreciable because acceleration of the fluid by buoyancy, near the surface, compensates for the deceleration of fluid by shear in the boundary layer along the test section wall. The support structure for the surface was designed to minimize drag, and the structural members were far away from the heated surface.

A regulated power supply was used to provide electrical power to the foil. During the experiment, the voltage was measured across the foil using a Hewlett Packard 3465B digital multimeter. The voltage was also measured across a Leeds and Northrup 0.01 ohm, 100 amp standard shunt in series with the foil, to determine the foil current. The foil current, and the voltage drop, were used to calculate the heat flux from the surface.

Velocity measurements were made using a Disa 55M01 constant-temperature hot wire anemometer with a Disa 55P14 miniature probe. The output from the anemometer was measured with a Hewlett Packard 3455A digital voltmeter. The hot-wire probe was L-shaped so that the wire was upstream of the probe support. This minimized probe support interference. The probe was calibrated in air using the test-rig of Shaukatullah [16]. This is a modification of the earlier apparatus of Dring and Gebhart [17]. The probe was calibrated at an overheat ratio of 1.6 for velocities up to 40 cm/s. The method described by Mahajan [18] was used to correct the hot-wire output for the effect of varying ambient temperature. A discussion of this correction method may also be found in Carey [19].

The boundary layer temperature measurements were made using a 0.0254 mm copper–constantan thermocouple. The two thermocouple leads were horizontal and parallel to the foil for about 0.8 cm on each side of the junction. In this arrangement, the wire lay essentially along an isotherm, reducing the conduction loss in the leads. These leads then passed through a pair of 1.0 mm hollow glass tubes which were attached to a support outside the boundary region. This support also held the hot-wire probe and the surface probe. The latter, a 1.5 mm copper rod, was used to locate the surface. The zero setting of the surface probe was obtained by connecting it through a resistance meter to the foil. The circuit was completed when the probe contacted the foil, causing the resistance reading to drop from an infinite value to some finite value. The relative positions of the thermocouple junction and hot-wire sensor with respect to this surface probe were determined from an enlarged photograph of the assembly. The hot-wire sensor, thermocouple junction and surface probe were in the same horizontal plane. The ambient air temperature in the tank was measured using a 0.0127 cm copper constantan thermocouple. An ice bath was used as a reference for both thermocouples. The output from the thermocouples was measured using a Hewlett Packard 3465B multimeter as a voltmeter.

The probe array was remotely traversed normal to the foil, in the boundary layer, using a Disa 55H01 traversing mechanism. This was driven by a Disa 52C01 stepper motor which was remotely controlled by a Disa 52B01 sweep drive unit. The output level corresponding to any given probe position was displayed with high accuracy on the three digit mechanical counter of the sweep drive unit. The probe could be accurately moved in steps of 0.203 mm. The distance of the probe from the leading edge was measured accurately before putting the assembly in the tank.

The thermocouple leads, the co-axial hot-wire cable and all the other electrical leads were taken out of the test section through sealed fittings in the side and top.

After turning on the air supply and applying the foil current, the flow was allowed about 2 min to reach steady state, for each test. Thermocouple and hot-wire readings were then taken at a number of points across the boundary layer. All measurements were taken at a single downstream location 31.4 cm above the lower edge of the surface. In each experiment, the convection heat flux was determined from the temperature measurements and power input to the foil. As described in Carey [19] the temperature measurements were used to correct for the weak effect of thermal radiation from the surface.

Temperature and velocity measurements were taken at the combinations of heat flux, q and free stream velocity, u_∞, listed in Table 2. The corresponding values of ε_M, ε_H and $\bar{R}$ for each of the combinations of u_∞ and q are also listed. The values of q and u_∞ listed in Table 2 were chosen to cover the widest possible range of $\bar{R}$ within the limits of the experimental set-up.

In Fig. 6, the measured velocity data is shown for each of the combinations of u_∞ and q in Table 2. Also shown, for each circumstance, are the calculated profiles from the analysis of the previous section. Excellent agreement is seen between the theoretical and experimental results. In Fig. 7, the measured temperature data is compared with the theoretical profiles for $(\varepsilon_M, \varepsilon_H) = (0, 0)$ and $(0.75, 0.028)$. Excellent agreement is again found between the calculations and the experimental data. In Fig. 8, the measured local overall temperature differences across the boundary region are shown, normalized with the value calculated for $\varepsilon_M = \varepsilon_H = 0$. Also shown is the calculated variation. The effect of ε_H, as seen in equation (40a) is much smaller than that of ε_M and is therefore neglected in Fig. 8. Note that for the uniform-flux surface

$$(t_o - t_\infty)/(t_o - t_\infty)_{\varepsilon_M=0} = (Nu_x)_{\varepsilon_M=0}/Nu_x.$$

The measured data in Fig. 8 is in very good agreement with the trend predicted by the analysis.

Table 2. The values of surface heat flux and free stream velocity at which velocity measurements were taken, the corresponding values of ε_M, ε_H and $\bar{R}$, and the symbols used in Figs. 6 and 7

q (W/m^2)	u_∞ (cm/s)	ε_M	ε_H	$\bar{R}$	Symbol
98.7	2.8	0.10	0.016	2.3	◆
26.0	4.0	0.27	0.020	5.0	▲
20.1	5.5	0.45	0.022	8.0	■
8.61	5.0	0.60	0.026	9.4	▼
5.64	5.2	0.75	0.028	11.1	◆

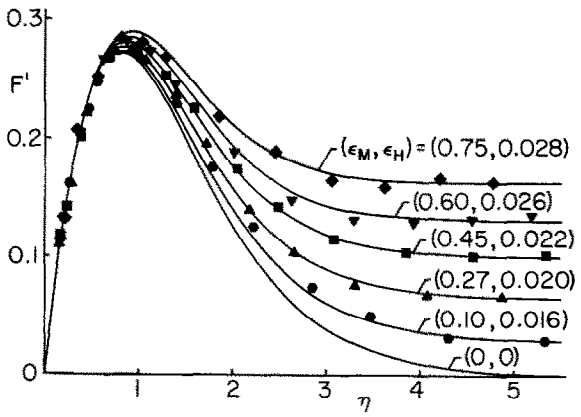

FIG. 6. Measured and theoretical velocity profiles for mixed convection flow along a vertical uniform-heat-flux surface in a uniform air stream. The experimental conditions corresponding to each symbol are listed in Table 2.

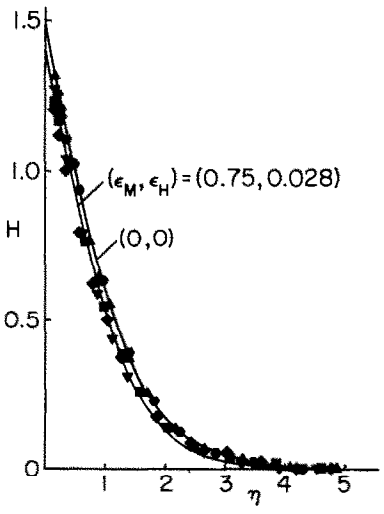

FIG. 7. Measured and theoretical temperature profiles for mixed convection flow along a vertical uniform-heat-flux surface in a uniform air stream. The experimental conditions corresponding to each symbol are listed in Table 2.

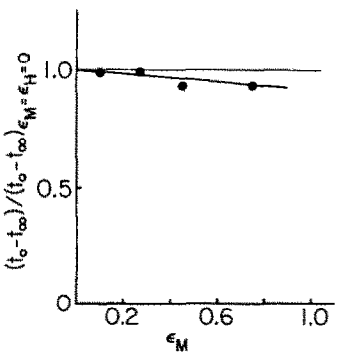

FIG. 8. Measured temperature differences (●) across the boundary layer for various ε_M. Also shown is the theoretical variation (——).

4. CONCLUSIONS

It has been shown that the method of matched asymptotic expansions can be used to simultaneously analyze non-boundary layer effects and the behavior of mixed convection at large downstream distances. For some conditions (small $\bar{R}$ and large ε_H), the first correction for higher-order boundary layer effects may be more important than the second correction for mixed convection effects. It is also seen that interaction of mixed convection and higher-order boundary layer effects produces cross terms in the expansions. Note also that if $\bar{R} \to 0$, the expansions reduce to those found by Mahajan and Gebhart [13], for higher-order boundary layer effects alone. If additional terms were included in the expansions, the next term to appear in the inner expansions would correspond to the 2nd-order correction for higher-order effects reported by Mahajan and Gebhart [13].

Measured temperature and velocity profiles are in excellent agrement with the predictions of the analysis. The measured effect of increasing ε_M, on the local overall temperature difference, was also found to agree with the results of the analysis.

Attention here has been focused mainly on assisting mixed convection effects. However, physical circumstances may arise in which strong buoyancy and weak free stream effects are opposed. Consider, for example, the flow circumstance shown in Fig. 9(a). A downward free stream flow exists over a vertical plate consisting of two sections. The lower portion is an impermeable uniform-heat-flux surface, which generates an upward buoyancy-driven flow along the surface. The upper portion of the plate is porous, and suction there completely absorbs the rising fluid in the upward wake above the heated portion of the surface.

Over most of the lower portion of the plate, strong buoyancy driven flow exists near the surface, with a weak outer downflow. From analysis, it is known that the buoyancy effect diminishes toward the lower edge of the plate. At some point near the lower edge, the buoyancy may be sufficiently small that the downward outside flow will dominate, and, through shear stress, produce a fully downward flow. The present analysis suggests that this will occur when $\varepsilon_M = \bar{R}/G^{*3/4} = O(1)$. Assuming a value of $\bar{R}$ of about 3, this implies $G^* = O(5)$. But $G^* = O(5)$ implies $\varepsilon_H = O(1)$. Hence, the present analysis implies that this inversion of the flow will occur extremely close to the lower edge of the plate, where boundary layer analysis is, in all events, inappropriate. Since non-boundary layer behavior near the leading edge does not have a strong effect farther up the plate, it is consistent to assume that this inversion will also have only a weak effect there. Actually there is no reason, *a priori*, to expect that this orderly variation of the velocity profile will cause the flow to deviate from the behavior predicted by the present analysis for $\bar{R} < 0$.

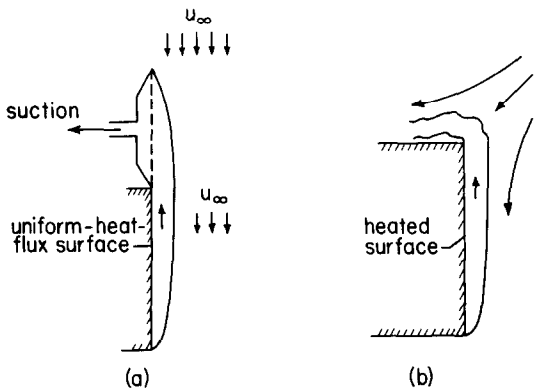

FIG. 9. Possible flow configurations resulting in opposed mixed convection flow.

These surmises are supported by the photographs of the flow near a vertical ice surface melting in cold pure water which were presented by Carey and Gebhart [20]. For an ambient water temperature, t_∞, of 4.7°C, the upward wake above the ice surface reverses due to the density extremum effects, and causes a downflow outside the upward flow near the ice surface. The flow for $t_\infty = 4.7$°C has exactly the characteristics of the flow in Fig. 9(a). Bi-directional flow exists over most of the surface, while near the lower edge, the flow is virtually all downward (see Fig. 2(d) of Carey and Gebhart [20]). The flow at higher locations on the surface apparently was not significantly affected by the flow condition near the lower edge.

The above considerations suggest that the analysis presented here may be applied to both aiding and, for some circumstances, opposed mixed convection. Since the expansions contain only integer powers of $\bar{R}$, opposed effects, corresponding to $\bar{R} < 0$, present no mathematical difficulties. While the flow in Fig. 9(a) is somewhat idealized, its behavior is similar to a more common flow situation, shown in Fig. 9(b). In this latter circumstances, fluid motion in the ambient, such as the wind, strikes the top corner of a heated vertical surface at an oblique angle. The wake is thereby deflected away to the left and an essentially vertical downward flow intereacts with an upward buoyancy driven flow near the surface. The present analysis may be a good approximate model for the transport along the heated surface in such circumstances. However, the expansions to $O(\bar{R}\varepsilon_H^{7/4})$ are not fully consistent for such opposed flows since they do not include higher-order effects associated with the top edge configuration. To obtain fully consistant higher-order approximations would require an analysis adapted to a specific trailing edge configuration.

Acknowledgements—The first author would like to acknowledge graduate fellowship support from the Graduate School at the State University of New York at Buffalo. The authors also wish to acknowledge support for this study by the National Science Foundation under research grant ENG77-21641.

REFERENCES

1. J. H. Merkin, The effect of buoyancy forces on the boundary-layer flow over a semi-infinite vertical flat

plate in a uniform free stream, *J. Fluid Mech.* **35**, 439–450 (1969).
2. S. Eshghy, Forced-flow effects on free-convection flow and heat transfer, *ASME J. Heat Transfer* **86**, 290–291 (1964).
3. A. A. Szewczyk, Combined forced and free-convection laminar flow, *ASME J. Heat Transfer* **86**, 501–507 (1964).
4. E. M. Sparrow and J. L. Gregg, Buoyancy effects in forced-convection flow and heat transfer, *ASME J. appl. Mech.* **26**, 133–134 (1959).
5. J. R. Kliegel, Laminar free and forced convection heat transfer from a vertical flat plate. Ph.D. thesis, University of California (1959).
6. J. R. Lloyd and E. M. Sparrow, Combined forced and free convection flow on vertical surfaces, *Int. J. Heat Mass Transfer* **13**, 434–438 (1970).
7. P. H. Oosthuizen and R. Hart, A numerical study of laminar combined convective flow over flat plates. Report 4/71, Thermal and Fluid Sciences Group, Queen's University, Kingston, Ontario, Canada (1971).
8. G. Wilks, Combined forced and free convection flow on vertical surfaces, *Int. J. Heat Mass Transfer* **16**, 1958–1964 (1973).
9. J. Gryzagoridis, Combined free and forced convection from an isothermal vertical plate, *Int. J. Heat Mass Transfer* **18**, 911–916 (1975).
10. M. J. Hommel, Mixed convection heat transfer from a vertical plate: Prandtl number effects. paper HT-17, presented at the ASME Winter Annual Meeting, New York (1976).
11. N. Afzal and N. K. Banthiya, Mixed convection over a semi-infinite vertical flat plate, *J. appl. Math. Phys. (ZAMP)* **28**, 993–1004 (1977).
12. G. Wilks, The flow of a uniform stream over a semi-infinite vertical flat plate with uniform surface heat flux, *Int. J. Heat Mass Transfer* **17**, 743–753 (1974).
13. R. L. Mahajan and B. Gebhart, Higher-order approximations to the natural convection flow over a uniform-flux vertical surface, *Int. J. Heat Mass Transfer* **21**, 549–556 (1978).
14. M. Van Dyke, *Perturbation Methods in Fluid Mechanics.* The Parabolic Press, Stanford, Calif. (1975).
15. K. Stewartson, On asymptotic expansions in the theory of boundary layers, *J. Math. Phys.* **36**, 173–191 (1957).
16. H. Shaukatullah, An experimental investigation of the natural convection boundary layer over a uniform flux inclined surface. Ph.D. dissertation, Cornell University (1977).
17. R. P. Dring and B. Gebhart, Hot wire anemometer calibration for measurements at very low velocity, *ASME J. Heat Transfer* **91**, 241–244 (1969).
18. R. P. Mahajan, Higher-order effects, stability and transition in vertical natural convection flows. Ph.D. dissertation, Cornell University (1977).
19. V. P. Carey, Transport in vertical mixed convection flows and natural convection flows in cold water. Ph.D. dissertation, State University of New York at Buffalo (1981).
20. V. P. Carey and B. Gebhart, Visualization of the flow adjacent to a vertical ice surface melting in cold pure water, *J. Fluid Mech.* **107**, 37–55 (1981).

TRANSPORT A GRANDE DISTANCE EN AVAL DANS UNE CONVECTION MIXTE ADJACENTE A UNE SURFACE VERTICALE A FLUX THERMIQUE UNIFORME

Résumé—On présente une analyse de perturbation de la convection mixte sur une surface verticale semi-infinie avec un flux thermique uniforme. Une technique de développement asymptotique est utilisée pour construire des développements interne et externe incluant, pour la première fois, à la fois la convection mixte et les effets de couche limite d'ordre élevé. On montre que ces effets peuvent être tous inclus pour obtenir des approximations d'ordre élevé pour l'écoulement de couche limite et de convection mixte à de grandes distances en aval. On présente des calculs numériques, pour $Pr = 0{,}733$ et 6, 7, qui indiquent les grandeurs relatives des effets de convection mixte et de non couche limite. De plus, de nouvelles mesures expérimentales de flux thermique surfacique, de profils de vitesse et de température sont présentées pour la convection mixte adjacente à une surface verticale chauffée à flux uniforme dans l'air. Les profils mesurés sont en bon accord avec ceux prévus par le calcul. La variation calculée du nombre de Nusselt est aussi conforme à celle déduite des mesures.

TRANSPORTVORGÄNGE IN DER AUSGEBILDETEN STRÖMUNG BEI GEMISCHTER KONVEKTION AN EINER SENKRECHTEN WAND MIT GLEICHFÖRMIGER WÄRMESTROMDICHTE

Zusammenfassung—Die gemischte Konvektion, die bei der Strömung über eine senkrechte halbunendliche Oberfläche mit gleichförmiger Wärmestromdichte auftritt, wird mit Hilfe der Störungs-Analyse untersucht. Eine angepaßte asymptotische Entwicklungs-Methode wird zur Darstellung der inneren und äußeren Funktionen verwendet, wobei erstmals sowohl Mischkonvektion als auch Grenzschicht-Effekte höherer Ordnung berücksichtig werden. Es wird gezeigt, daß diese Effekte simultan berücksichtigt werden müssen, um konsistente Approximationen höhere Ordnung für die gemischte Konvektion in der ausgebildeten Grenzschichtströmung zu erhalten. Numerische Berechnungen werden für $Pr = 0{,}733$ und 6,7 angegeben; diese zeigen die relativen Größenordnungen der gemischten Konvektion und der Nicht-Grenzschicht-Effekte. Darüber hinaus wird über neue experimentelle Messungen des Wärmeübergangs und der Geschwindigkeits- und Temperaturprofile für gemischte Konvektion in einer Luftströmung an einer senkrechten Wand mit gleichförmiger Wärmestromdichte berichtet. Die gemessenen Profile zeigen eine vorzügliche Übereinstimmung mit den vorausberechneten. Ebenso stimmt der vorausberechnete Verlauf der Nusselt-Zahl gut mit den Werten überein, die sich aus den Messungen ergeben.

ПЕРЕНОС НА БОЛЬШИХ РАССТОЯНИЯХ ВНИЗ ПО ПОТОКУ ПРИ ТЕЧЕНИИ СО СМЕШАННОЙ КОНВЕКЦИЕЙ У ВЕРТИКАЛЬНОЙ РАВНОМЕРНО НАГРЕВАЕМОЙ ПОВЕРХНОСТИ

Аннотация — Методом возмущений исследовано течение при смешанной конвекции у вертикальной полубесконечной равномерно нагреваемой поверхности. Для построения внутренних и внешних разложений с учетом (что было выполнено впервые) влияния как смешанной конвекции, так и пограничного слоя в приближении высшего порядка, используется соответствующий метод асимптотического разложения. Показано, что получение согласованных приближений высшего порядка для погранслойного течения при смешанной конвекции на больших расстояниях вниз по потоку требует одновременного учета этих эффектов. Численные расчеты представлены для значений числа Прандтля, равных $Pr = 0{,}733$ и 6,7 и отражающих относительный вклад смешанной конвекции и эффектов, не учитываемых пограничным слоем. Кроме того, представлены новые результаты экспериментального измерения интенсивности переноса тепла на поверхности, а также профилей скорости и температуры для течения со смешанной конвекцией у вертикальной равномерно нагреваемой поверхности в воздухе. Измеренные профили хорошо согласуются с расчетными. Показано также хорошее совпадение рассчитанных и измеренных значений числа Нуссельта.